Electrochemical Supercapacitive Performance of Spray-Deposited NiO Electrodes

Abhijit A. Yadav & U. J. Chavan

Journal of Electronic Materials

ISSN 0361-5235
Volume 47
Number 7

Journal of Elec Materi (2018)
47:3770-3778
DOI 10.1007/s11664-018-6243-4

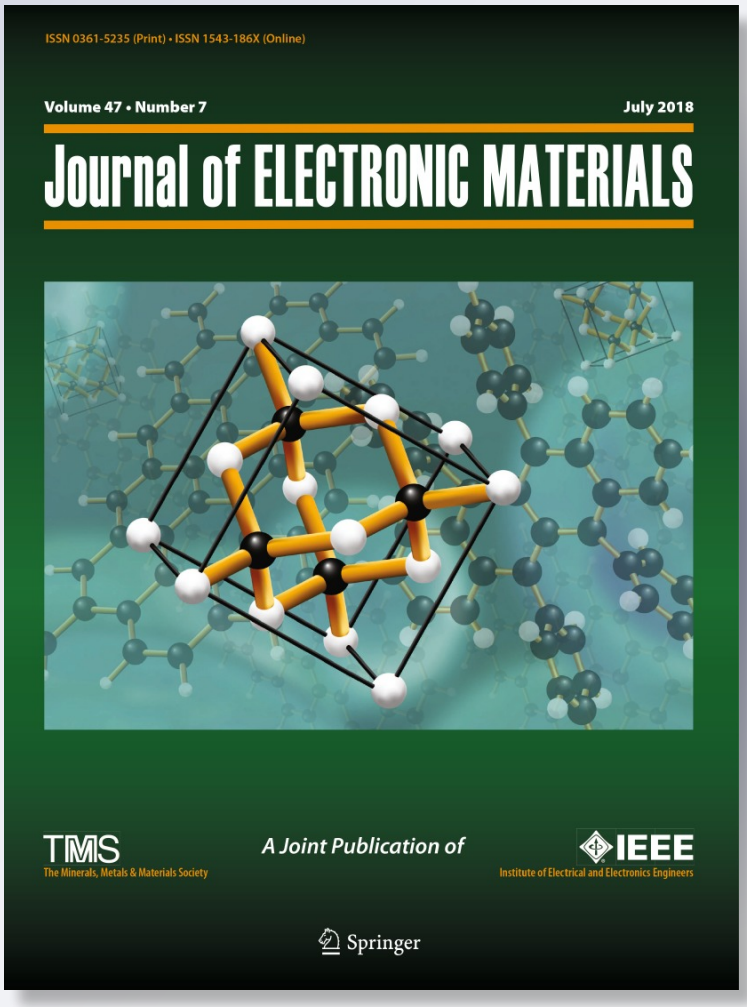

Springer

Journal of ELECTRONIC MATERIALS, Vol. 47, No. 7, 2018
https://doi.org/10.1007/s11664-018-6243-4

Electrochemical Supercapacitive Performance of Spray-Deposited NiO Electrodes

ABHIJIT A. YADAV [1,2] and U.J. CHAVAN[1]

1.—Thin Film Physics Laboratory, Department of Physics, Electronics and Photonics, Rajarshi Shahu Mahavidyalaya, Latur (Autonomous), Latur 413512, Maharashtra, India. 2.—e-mail: aay_physics@yahoo.co.in

Transition-metal oxides with porous structure are considered for use as promising electrodes for high-performance supercapacitors. Nanocrystalline nickel oxide (NiO) thin films have been prepared as active material for supercapacitors by spray pyrolysis. In this study, the effects of the film thickness on its structural, morphological, optical, electrical, and electrochemical properties were studied. X-ray diffraction analysis revealed cubic structure with average crystalline size of around 21 nm. Scanning electron microscopy showed porous morphology. The optical bandgap decreased from 3.04 eV to 2.97 eV with increase in the film thickness. Electrical resistivity measurements indicated semiconducting behavior. Cyclic voltammetry and galvanostatic charge/discharge study revealed good pseudocapacitive behavior. Specific capacitance of 564 F g^{-1} at scan rate of 5 mV s^{-1} and 553 F g^{-1} at current density of 1 A g^{-1} was observed. An NiO-based supercapacitor delivered specific energy of 22.8 W h kg^{-1} at specific power of 2.16 kW kg^{-1}, and retained 93.01% specific capacitance at current density of 1 A g^{-1} after 1000 cycles. Therefore, taking advantage of the porous morphology that exists in the nanostructure, such NiO materials can be considered for use as promising electrodes for high-performance supercapacitors.

Key words: Nanostructured materials, X-ray diffraction, crystal structure, scanning electron microscopy, energy storage materials, electrochemical impedance spectroscopy

INTRODUCTION

With development of the world economy, exhaustion of global energy will become unavoidable at the current rate of energy consumption. It is predicted that our global energy requirements will double by the middle of the century and triple by 2100.[1] Thus, there is an ever-growing and crucial need for development of renewable and alternative energy sources as well as energy conversion and storage systems.[2,3] Among various promising methods for energy storage, some of the most practical systems are fuel cells, secondary batteries, and capacitors,[4–6] each having its own characteristics and advantages. Electrochemical capacitors or supercapacitors are the most significant storage devices due to their high power and energy density combined with excellent cycle stability.[7] Supercapacitors can broadly be classified into electric double-layer capacitors (EDLCs) and pseudocapacitors. In an EDLC, energy storage occurs without involvement of charge transfer from the electrode surface to an electrolyte, while a pseudocapacitor stores energy based on charge transfer produced by Faradaic reactions.[8] Supercapacitors are utilized in diverse applications ranging from hybrid electric vehicles, memory backup, military and space equipment to wearable electronics, paper-like electronics, and flexible biomedical devices.[9,10] The challenge lies in development of devices that can store more energy at high power and energy density.

(Received September 4, 2017; accepted March 17, 2018; published online April 2, 2018)

At present, activated carbon, conductive polymers, and transition-metal oxides are commonly used as electrode materials in EDLCs.[11] Amongst these, metal oxides are cost effective, readily available, and simple to synthesize. Also, they show different redox states, which is useful for pseudocapacitors.[12] RuO_2 shows remarkable electrochemical performance with high specific capacitance.[13] However, its high cost and limited abundance limit industrial applications. Besides RuO_2, other metal oxides such as cobalt oxide,[14] nickel oxide,[15] manganese oxide,[5] iron oxide,[2,16] tin oxide,[17] zinc oxide,[18] and copper oxide[4,19] are also used as electrode materials. Nickel oxide (NiO) is one of the most promising electrodes for supercapacitors. NiO shows pseudocapacitive behavior with superior specific capacitance.[20]

Zeng et al.[21] synthesized porous NiO nanostructures via a solvothermal route, reporting specific capacitance of 532 F g^{-1} at current density of 2 A g^{-1}. Hydrothermally prepared NiO nanosheets possessing specific capacitance of 81.76 F g^{-1} at current density of 0.5 A g^{-1} were reported by Xiao et al.[22] NiO hierarchical hollow nanofibers with porous fiber-like morphology were synthesized through a simple ion-exchange process, showing specific capacitance of 700 F g^{-1} at current density of 2 A g^{-1} and 96% retention of specific capacitance after 5000 cycles at current density of 5 A g^{-1}.[23] Yu et al.[24] synthesized porous NiO nanosheets and observed capacitance of 600 F g^{-1} after 1000 cycles at high current density of 10 A g^{-1}. Specific capacitance of 128 F g^{-1}, 60 F g^{-1}, 146.3 F g^{-1}, and 129.5 F g^{-1} was reported for NiO films prepared by template method, precipitation synthesis, electrodeposition, and chemical route, respectively.[25] Jing et al.[26] synthesized NiO quantum dots embedded with few-layer exfoliative graphene, showing specific capacitance of 1181.1 F g^{-1} at current density of 2.1 A g^{-1}.

NiO films can be prepared by various techniques, including atomic layer deposition, sputtering, electron beam evaporation, pulsed laser deposition, hydrothermal methods, chemical bath deposition, sol–gel approaches, and spray pyrolysis.[27–29] Amongst these, spray pyrolysis is a simple, inexpensive, and readily applicable deposition method. The different precursors used for preparation of NiO thin films include nickel chloride, nickel acetate, nickel nitrate, and nickel formate-ethylenediamine.[27,30,31] Also, different substrates including nickel foam, graphene layer, steel, fluorine-doped tin oxide (FTO), indium-doped tin oxide (ITO), copper, quartz, and alumina were used in literature studies.[32–34] From a brief literature survey, and to the best of the authors' knowledge, there are few reports on preparation of NiO films using mixed aqueous/organic solvent. Therefore, in the present study, NiO films with various thicknesses were deposited by spray pyrolysis using aqueous/organic solvent mixture, and their electrochemical properties were studied.

EXPERIMENTAL PROCEDURES

NiO electrodes were successfully deposited onto amorphous and FTO-coated glass substrates using a computerized chemical spray pyrolysis technique discussed elsewhere.[35] Precursor solution was prepared by mixing 0.5 M nickel chloride hexahydrate ($NiCl_2{\cdot}6H_2O$) and isopropyl alcohol (1:1 volume ratio) prior to deposition. The film thickness was varied by spraying various different quantities of solution, viz. 15 cm^3, 20 cm^3, 25 cm^3, and 30 cm^3, respectively. Other process parameters were kept constant at their optimized value. Air was used as carrier gas at pressure of 1.8 kg cm^{-2}. The substrate temperature was kept constant at 450°C, the spray nozzle to substrate distance was fixed at 30 cm, and the spray rate employed was 3 mL min^{-1}.

NiO thin films were characterized by x-ray diffraction (XRD) analysis, scanning electron microscopy (SEM), optical and electrical resistivity measurements, and electrochemical analysis. Structural properties were studied by x-ray diffractometer using Cu K_α radiation. Surface morphology was studied by SEM. The optical bandgap was determined from absorption spectra recorded by ultraviolet–visible (UV–Vis) spectrophotometer. Electrical resistivity was measured by direct-current (DC) two-point probe method. Electrochemical performance was tested by cyclic voltammetry (CV), galvanostatic charge/discharge (GCD) measurements, and electrochemical impedance spectroscopy (EIS) using an electrochemical analyzer with 2 M aqueous KOH solution as electrolyte. CV study was carried out in the potential range from 0.15 V to 0.45 V versus Ag/AgCl at different scan rates. GCD measurements were carried out at various current densities. EIS measurements were performed at alternating-current (AC) amplitude of 5 mV in the frequency range from 100 kHz to 1 Hz.

RESULTS AND DISCUSSION

Film Thickness

$NiCl_2{\cdot}6H_2O$ was used as starting material for deposition of NiO thin films. Precursor solution was sprayed onto substrates preheated to 450°C. Overall, the chemical reaction involves decomposition of $NiCl_2{\cdot}6H_2O$ to NiO. The possible chemical reaction can be expressed as

$$NiCl_2 6H_2O \rightarrow NiO + 2HCl\uparrow + 5H_2O\uparrow \qquad (1)$$

A similar reaction was reported previously for spray-deposited NiO thin films by Sharma et al.[36] The as-deposited NiO thin films were greenish, uniform, and well adherent. Film thickness was calculated by the gravimetric weight difference

method, assuming a bulk density of NiO of $\rho = 6.67$ g cm^{-3}, as

$$t = \frac{\Delta m}{\rho \times l \times b}, \quad (2)$$

where t is the film thickness, Δm is the mass difference, ρ is the bulk density of the material, and $(l \times b)$ is the area of the NiO film. The thickness of the spray-deposited NiO films was found to be 350 nm, 402 nm, 470 nm, and 520 nm when depositing 15 cm^3, 20 cm^3, 25 cm^3, and 30 cm^3 spraying solution, respectively, with corresponding mass loading of 0.23 mg cm^{-2}, 0.27 mg cm^{-2}, 0.31 mg cm^{-2}, and 0.35 mg cm^{-2}. Initially, the film thickness increased linearly up to 470 nm with increasing quantity of spraying solution, then started to saturate thereafter. This initial rise in film thickness can be ascribed to supply of more constituent ions with increasing quantity of spraying solution. The saturation of the film thickness when applying more than 25 cm^3 spraying solution is due to partial thermal decomposition of the spray solution. Similar behavior was reported previously for spray-deposited F:SnO_2 thin films.[37]

XRD Analysis

Structural analysis of spray-deposited NiO thin films was carried out by XRD using Cu K_α radiation in the 2θ range from 10° to 90°. Figure 1 shows XRD patterns of NiO films with various thicknesses. Peaks were observed at 2θ angles of 37.53°, 43.46°, 62.87°, 75.44°, and 79.55°, corresponding to (111), (200), (220), (311), and (222) planes, respectively. Comparison of the calculated and standard d values from Joint Committee on Powder Diffraction Standards (JCPDS) data card 47-1049 indicated cubic crystal structure. No other diffraction peaks associated with Ni_2O_3, $Ni(OH)_2$ or NiOOH were observed, indicating formation of NiO. The interplanar spacing (d) values obtained from Bragg's condition matched well with standard values, as presented in Table I. The lattice parameter (a) was calculated using the relation[38]

$$d^2 = \frac{a^2}{(h^2 + k^2 + l^2)}, \quad (3)$$

where d is the interplanar spacing and h, k, l are the Miller indices. The average lattice parameter for cubic NiO was found to be $a = 4.1657$ Å. From Fig. 1, it is observed that the peak intensity increased with increase in the film thickness, and the peak observed at $2\theta = 37.53°$ had the highest intensity, indicating preferential (111) growth of the NiO thin films.

The crystalline size was calculated for the (111) plane using the Debye–Scherrer equation, given elsewhere.[39] It was found that the crystalline size varied slightly with the film thickness. The average crystalline size was found to be 21 nm, in good agreement with the values of 19 nm to 20 nm reported by Sharma et al.[36] for spray-deposited Zn-doped NiO thin films and 12 nm to 24 nm reported by Gowthami and coworkers for spray-pyrolyzed NiO thin films.[40] Table I summarizes the peak positions, calculated d values, lattice parameter a, and crystalline size of the NiO thin films.

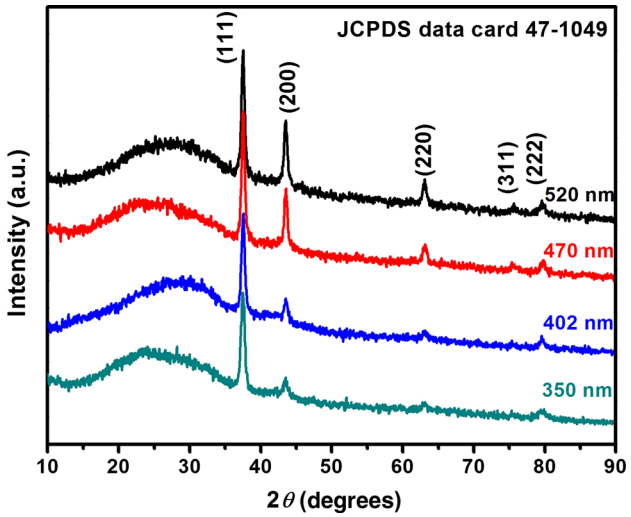

Fig. 1. XRD patterns of spray-deposited NiO thin films with various thicknesses.

Surface Morphology

Figure 2 shows SEM images of NiO thin films at magnification of 5000×. The SEM results show that the films were porous. Large numbers of small pores were clearly observed on the NiO surface. The pores were inhomogeneous in nature. The film porosity increased with increasing film thickness. Smaller pores enhance the electrode–electrolyte contact area and favor electrochemical reactions. An open mouth can also be noted in Fig. 2, suggesting that the NiO films had hollow nature. Such hollow architectures can reduce the diffusion lengths of electrolyte ions in the electrode and suppress the volume change during the cycling process, thus enabling durable high-rate capability.[41] Such porous morphology is favorable for Faradaic surface reactions, as it facilitates access of ions at the electrode–electrolyte interface. Similar porous morphology was observed by Inamdar et al.[25] for chemically grown NiO thin films.

Optical Measurements

Figure 3 shows the variation of $(\alpha h\upsilon)^2$ versus $h\upsilon$ for spray-deposited NiO thin films. The optical bandgap of the NiO thin films was estimated using the Tauc relation, given elsewhere,[38] by extrapolating the straight-line portion of the $(\alpha h\upsilon)^2$ versus $h\upsilon$ plots to the energy axis. It was observed that the optical bandgap decreased from 3.04 eV to 2.97 eV as the film thickness increased from 350 nm to

Table I. Structural properties of spray-deposited NiO thin films

t (nm)	2θ (°)	d_{cal} (Å)	d_{std} (Å)	(hkl)	a_{cal} (Å)	a_{std} (Å)	D (nm)
350	37.53	2.396	2.412	111	4.149	4.176	20
	43.46	2.082	2.088	200	4.163		
	62.93	1.476	1.477	220	4.176		
	75.44	1.259	1.259	311	4.177		
	79.70	1.203	1.206	222	4.166		
402	37.55	2.394	2.412	111	4.147	4.183	21
	43.50	2.079	2.088	200	4.159		
	62.87	1.477	1.477	220	4.179		
	75.34	1.260	1.259	311	4.178		
	79.54	1.205	1.206	222	4.173		
470	37.53	2.396	2.412	111	4.149	4.170	22
	43.58	2.076	2.088	200	4.152		
	62.87	1.477	1.477	220	4.179		
	75.34	1.260	1.259	311	4.178		
	79.40	1.207	1.206	222	4.179		
520	37.53	2.395	2.412	111	4.149	4.168	19
	43.54	2.078	2.088	200	4.156		
	63.10	1.473	1.477	220	4.166		
	75.46	1.259	1.259	311	4.176		
	79.56	1.204	1.206	222	4.172		

t, film thickness; 2θ, Bragg's angle; d, interplanar spacing; hkl, Miller indices; a, lattice parameter; D, crystalline size.

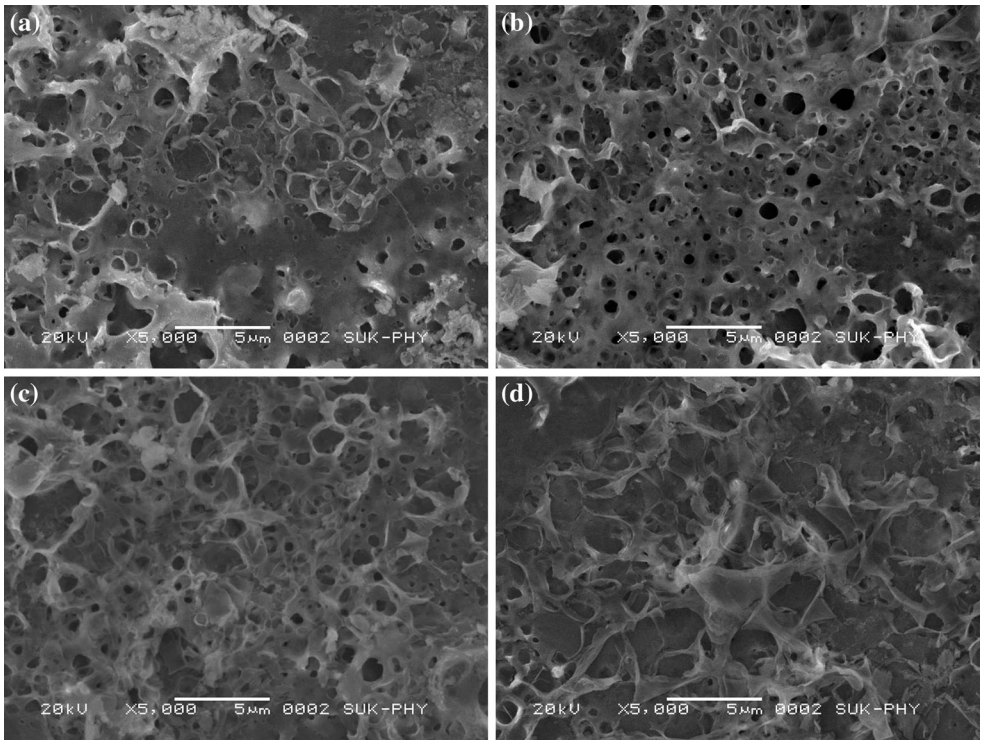

Fig. 2. SEM images (5000× magnification) of spray-deposited NiO thin films with thickness of (a) 350 nm, (b) 402 nm, (c) 470 nm, and (d) 520 nm.

520 nm. These values are lower than the reported values of 3.15 eV to 3.80 eV[42] and 3.37 eV to 3.76 eV for NiO films.[43] The red-shift observed in the bandgap compared with the bulk value may be due to larger grain sizes or deep states introduced in the bandgap of the NiO compound. A similar red-shift in the bandgap was reported by Yung and coworkers[44] for Sn-doped ZnO films obtained using the sol-gel method. The decrease in bandgap with increasing film thickness may be related to changes

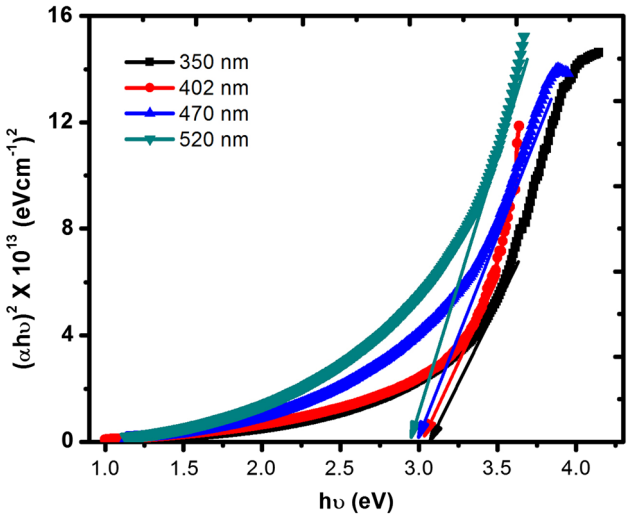

Fig. 3. Variation of $(\alpha h\upsilon)^2$ versus $h\upsilon$ for spray-deposited NiO thin films with various thicknesses.

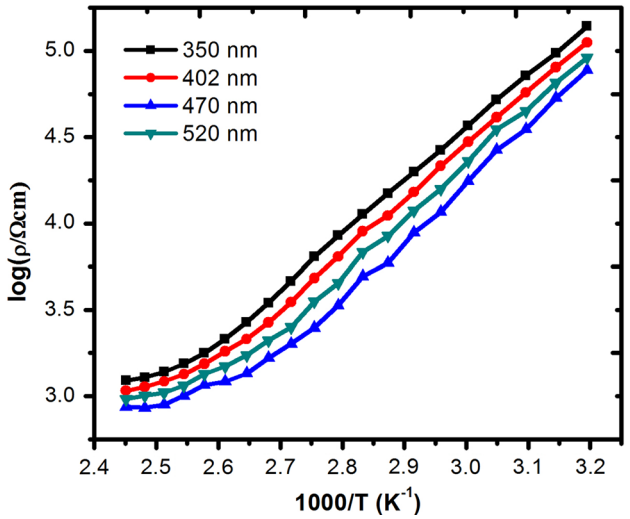

Fig. 4. Variation of logρ with inverse absolute temperature for spray-deposited NiO thin films with various thicknesses.

in homogeneity and film crystallinity, caused by differences in experimental conditions, such as the quantity of spraying solution applied, the spray rate, and substrate cooling during deposition.[40]

Electrical Resistivity

Figure 4 shows the variation of log ρ as a function of inverse absolute temperature for the NiO thin films. It was observed that the film resistivity decreased with rise in temperature, confirming typical semiconducting behavior. The electrical resistivity found for the NiO thin films was on the order of 10^4 Ω cm, much lower than the value of 10^{13} Ω cm for stoichiometric NiO thin films.[45] The electrical resistivity of NiO films mainly depends on their microstructural defects, composition, and annealing treatment. The low electrical resistivity observed in the present study is due to formation of nonstoichiometric NiO films. Nonstoichiometric NiO has excess oxygen or nickel deficiency, hence decreasing the resistivity.[45,46] The variation of the electrical resistivity with temperature can be attributed to improved crystallization.[47] The decrease in electrical resistivity with film thickness can be ascribed to surface scattering and increased carrier concentration. At lower thickness, more defects act as scattering centers, forming trapping centers that minimize the free carriers available for conduction.[48]

The activation energy of the NiO films, calculated using the Arrhenius relation,[35] lay in the range of 0.279 eV to 0.3 eV and 0.027 eV to 0.142 eV in the low- and high-temperature regions, respectively, in good agreement with the values of 0.08 eV to 0.14 eV reported by Hakim et al.[49] for spray-deposited NiO thin films. This variation of the activation energy with film thickness can be understood based on island structure theory.[50]

Electrochemical Measurements

CV

CV analysis of NiO films was performed using 2 M KOH electrolyte at different scan rates within the potential window from 0.15 V to 0.45 V versus Ag/AgCl, matching well with the window of 0.05 V to 0.55 V for NiO nanoflakes reported by Zhu et al.[33] Figure 5a–d shows the CV results obtained at different scan rates for spray-deposited NiO thin films with various thicknesses. A pair of redox peaks is observed during the anodic and cathodic sweeps, indicating pseudocapacitance. The specific capacitance, C_{sp}, was calculated using the relation given elsewhere.[5] The specific capacitance values for the different film thicknesses are presented in Table II. The maximum specific capacitance of 564 F g^{-1} at scan rate of 5 mV s^{-1} was obtained for the film with thickness of 470 nm.

The effect of the scan rate on the specific capacitance is shown in Fig. 6a. As the scan rate was increased, the specific capacitance decreased due to partial charge transfer from the electrolyte to electrode at higher scan rates.[51] Figure 6b shows the variation of the specific capacitance with the film thickness. The specific capacitance increased with increase in the film thickness, reaching a maximum of 564 F g^{-1} at 470 nm but decreasing thereafter. This behavior can be attributed to enhancement of the surface area and porosity of the films, as observed by SEM. At higher thickness (520 nm), a fall in the specific capacitance is observed due to the increase in the deposited mass. The specific capacitance observed in the present study is higher than the value of 385.5 F g^{-1} at 5 mV s^{-1} reported by Cao et al.[20] for pure NiO. Specific capacitance of 167 F g^{-1} in 2 M KOH was reported by Patil et al.[28] for chemically deposited nanocrystalline NiO thin films. Navale and coworkers reported specific

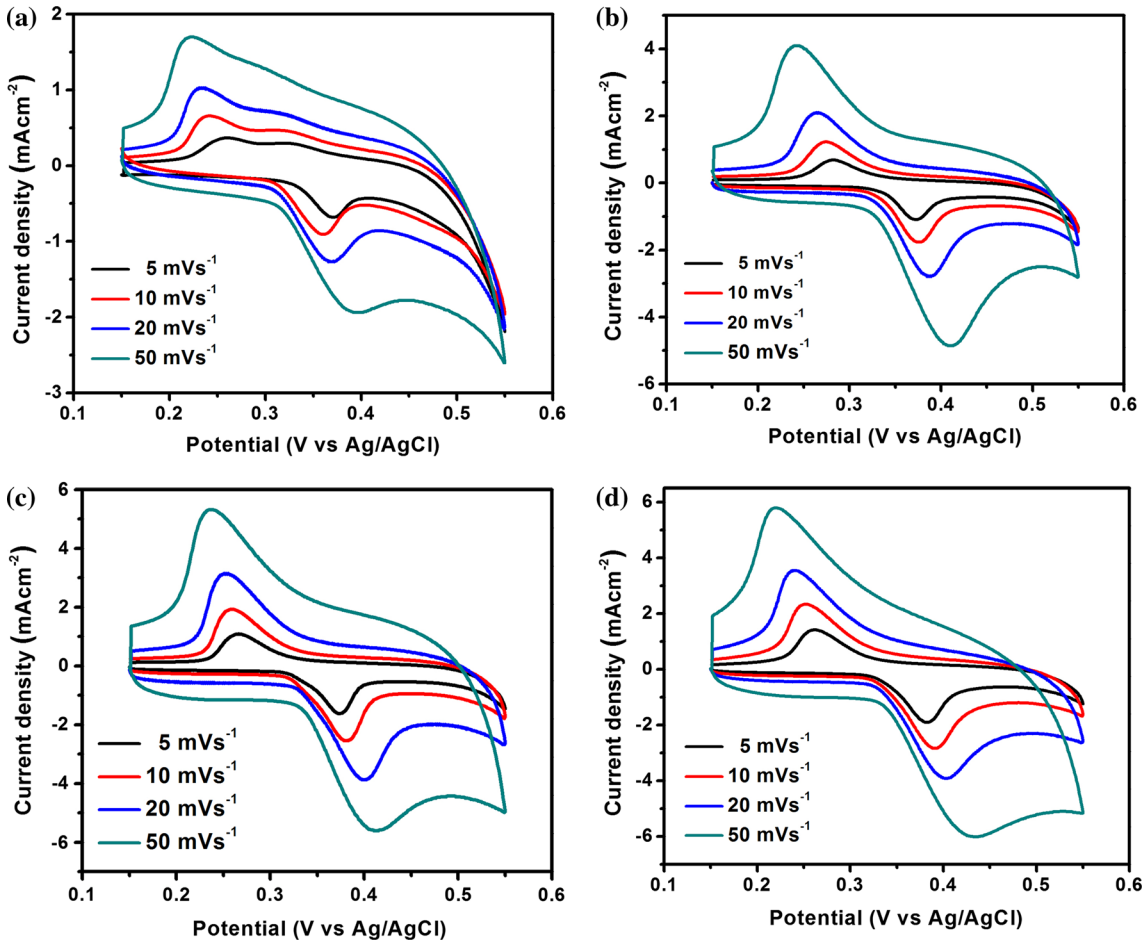

Fig. 5. CV results obtained at different scan rates for spray-deposited NiO thin films with thickness of (a) 350 nm, (b) 402 nm, (c) 470 nm, and (d) 520 nm.

Table II. Optical, electrical, and electrochemical properties of spray-deposited NiO thin films

		Activation energy (eV)				
t (nm)	E_g (eV)	HT	RT	C_{sp} (F g^{-1})	R_s (Ω)	R_{ct} (Ω cm^2)
350	3.04	0.110	0.300	405	0.35	10.05
402	3.01	0.142	0.279	466	0.32	9.75
470	2.99	0.027	0.291	564	0.25	7.50
520	2.97	0.053	0.295	529	0.30	8.90

t, film thickness; E_g, optical bandgap energy; C_{sp}, specific capacitance from CV; R_s, solution resistance; Rct, charge-transfer resistance; *RT*, room temperature; *HT*, high temperature.

capacitance of 458 F g^{-1} at scan rate of 5 mV s^{-1}[52] for NiO synthesized on steel substrate using a conventional three-electrode electrochemical cell.

GCD

Figure 7a shows the GCD curves obtained at current density of 1 A g^{-1} for NiO electrodes with different film thicknesses. As seen from this figure, the discharge curves show significant deviation from a straight, flat line, indicating that the capacitance mainly originates from Faradaic redox reactions. This suggests typical pseudocapacitive behavior[28] as a result of the electrochemical redox reaction occurring at the electrode–electrolyte interface of the NiO electrodes, in good agreement with

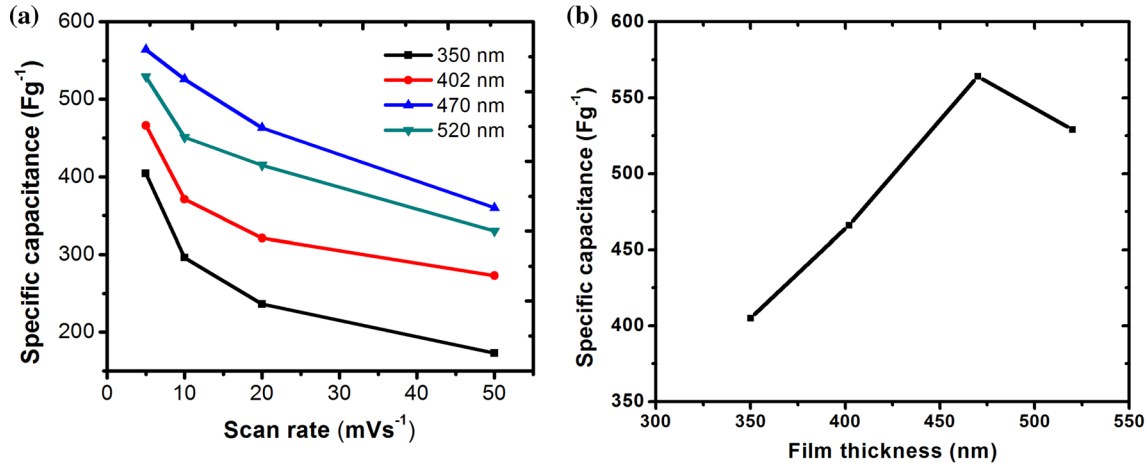

Fig. 6. Variation of specific capacitance with (a) scan rate for spray-deposited NiO thin films with various thicknesses and (b) film thickness for NiO thin films.

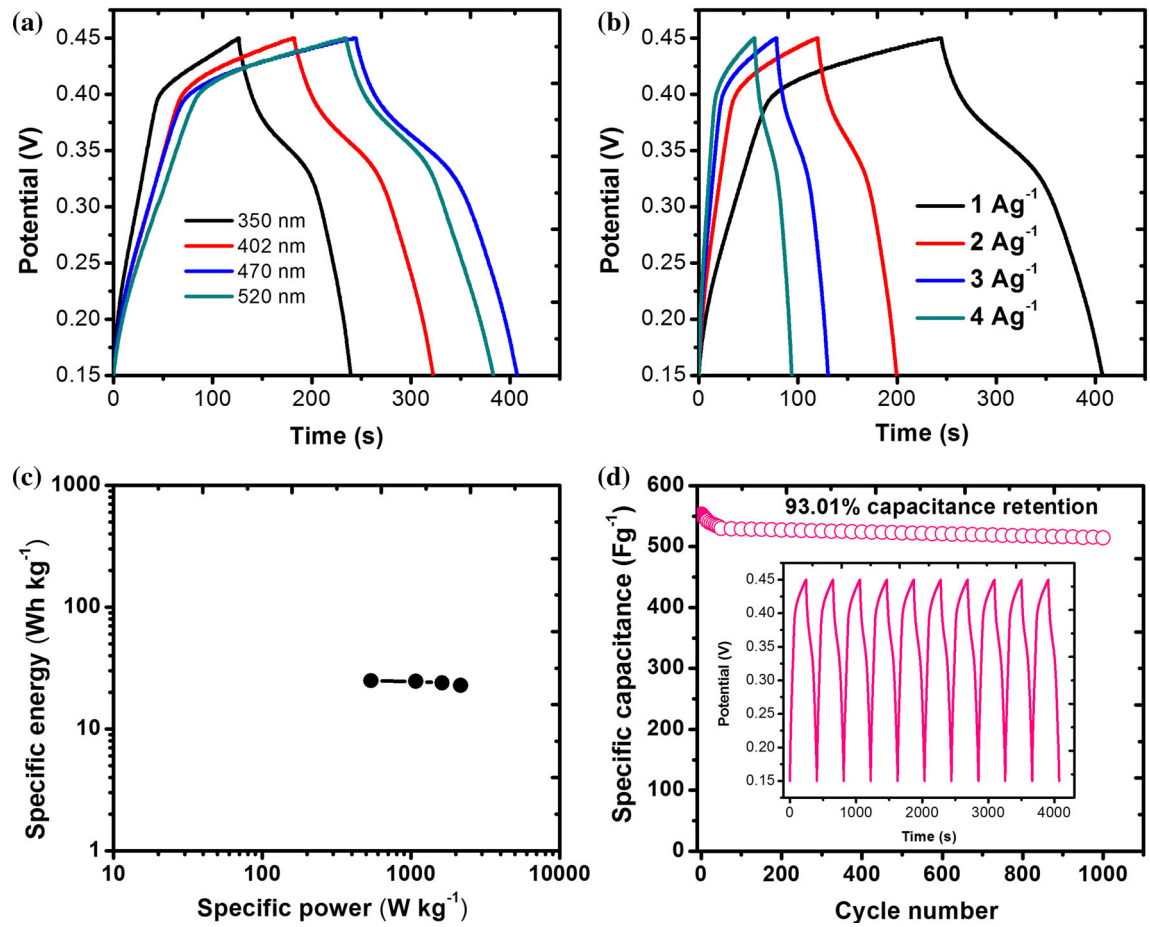

Fig. 7. (a) GCD curves for NiO electrodes with various film thicknesses obtained at current density of 1 A g^{-1}. (b) GCD curves for NiO thin-film electrode (470 nm) supercapacitor at different current densities. (c) Ragone plots for NiO thin-film electrode supercapacitor with film thickness of 470 nm. (d) Cycling performance of NiO thin-film electrode (470 nm) at current density of 1 A g^{-1}. Inset shows charge/discharge curves for the first 10 cycles.

the CV results. The specific capacitance (C_{sp}, F g^{-1}), specific energy (SE, W h kg^{-1}), and specific power (SP, kW kg^{-1}) were calculated using relations given elsewhere.[53,54] The specific capacitance for the NiO electrodes was found to be 380 F g^{-1}, 474 F g^{-1}, 553 F g^{-1}, and 503 F g^{-1} for film thickness of

Table III. Various parameters for obtaining specific capacitance, specific energy, and specific power from GCD measurements

CD (A g^{-1})	t_{dis} (s)	C_{sp} (F g^{-1})	SE (W h kg^{-1})	SP (kW kg^{-1})
1	166	553	24.90	0.54
2	82	547	24.60	1.08
3	53	530	23.85	1.62
4	38	507	22.80	2.16

CD, current density; t_{dis}, discharge time; C_{sp}, specific capacitance from GCD; *SE*, specific energy; *SP*, specific power.

350 nm, 402 nm, 470 nm, and 520 nm, respectively. The maximum specific capacitance of 553 F g^{-1} obtained at current density of 1 A g^{-1} is much higher than the value of 81.76 F g^{-1} at current density of 1 A g^{-1} reported by Xiao et al.[22] for NiO nanosheets synthesized by a hydrothermal process, 110 F g^{-1} at current density of 0.1 A g^{-1} recently reported by Duraisamy et al.[55] for binder-free NiO, and 260 F g^{-1} at current density of 1 A g^{-1} for NiO prepared by an ultrasonic method.[56] Figure 7b shows the GCD curves obtained for a supercapacitor with a NiO electrode (thickness 470 nm) at different current densities.

The variation of the specific energy with the specific power (Ragone plot) is shown in Fig. 7c. The specific energy was found to be 24.90 W h kg^{-1} with specific power of 540 W kg^{-1} at constant current density of 1 A g^{-1}. The values of specific power and specific energy obtained at different current densities are presented in Table III.

To evaluate the stability, the cycle performance of the NiO electrode was examined through cycle charge/discharge testing at current density of 1 A g^{-1}, as shown in Fig. 7d. The inset shows the charge/discharge curves of the first 10 cycles of the NiO electrode. After 1000 charge/discharge cycles, the electrode showed an overall decay of $\sim$ 6.99%, confirming its high structural stability. These results indicate that the NiO electrode exhibited good electrochemical stability and reversibility.

EIS

Figure 8 shows the Nyquist plots of NiO electrodes with different film thicknesses, while the inset shows an enlargement of the high-frequency region. The EIS spectra can be divided into three regions based on the frequency. The curve shows vertical lines in the low-frequency region, being characteristic of supercapacitive behavior, and inclined Warburg-like curves at high frequencies, indicating typical electric double-layer behavior.[31] The semicircle in the high-frequency region shows internal resistance and charge-transfer resistance. From the Nyquist plots, it is seen that the electrolyte resistance (R_s) and charge-transfer resistance (R_{ct}) lay in the ranges of 0.25 Ω to 0.35 Ω and 7.5 Ω cm^2 to 10.05 Ω cm^2, respectively. Table II presents the values of R_s and R_{ct} for supercapacitors

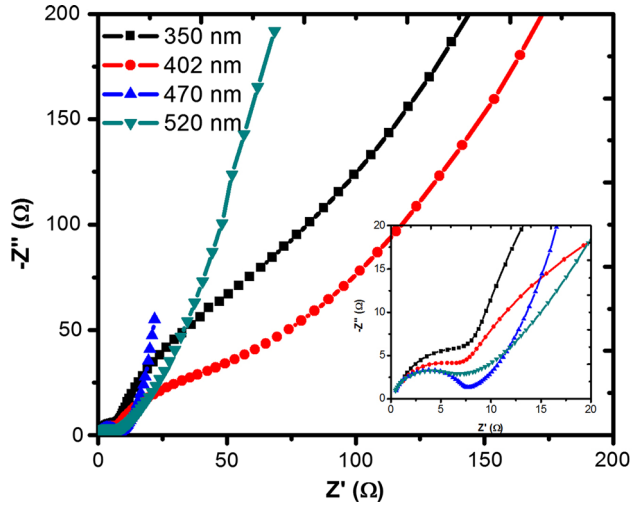

Fig. 8. Nyquist plots for spray-deposited NiO thin films with various thicknesses. Inset shows enlarged view in high-frequency region.

formed using NiO films with various thicknesses. The low electrolyte resistance and charge-transfer resistance are beneficial for electrochemical supercapacitor applications.

CONCLUSIONS

NiO thin films with different thicknesses were deposited by spray pyrolysis, exhibiting cubic crystal structure with average lattice parameter of 4.16 Å. Small pores were clearly observed on the NiO film surface by SEM. Film porosity increased with increase in the film thickness. The optical bandgap decreased as the film thickness increased. The room-temperature electrical resistivity was found to be on the order of 10^4 Ω cm. Superior electrochemical performance was observed, including high specific capacitance and good cycle stability, reaching 564 F g^{-1} with retention ratio of about 93.01% after 1000 cycles at 1 A g^{-1}. This work not only provides a promising pseudocapacitive material but also highlights a route towards next-generation energy storage devices.

ACKNOWLEDGEMENT

This research is financially supported by the Science and Engineering Research Board, Department of Science and Technology, New Delhi, India

through the Project under SERC Fast Track Scheme for Young Scientist to Abhijit A. Yadav (File No. SB/FTP/PS-068/2013).

REFERENCES

1. J. Yan, Q. Wang, T. Wei, and Z. Fan, *Adv. Energy Mater.* 4, 11 (2014).
2. T.P. Tran and Q.H. Do, *J. Electron. Mater.* 46, 6056 (2017).
3. B. Wang, J. Qiu, H. Feng, E. Sakai, and T. Komiyama, *J. Electroanal. Chem.* 775, 219 (2016).
4. N.H. Alshareef, D. Whitehair, and C. Xia, *J. Electron. Mater.* 46, 1628 (2017).
5. A.A. Yadav, S.N. Jadhav, D.M. Chougule, P.D. Patil, U.J. Chavan, and Y.D. Kolekar, *Electrochim. Acta* 206, 134 (2016).
6. W. Dang, C. Dong, Z. Zhang, G. Chen, Y. Wang, and H. Guan, *Electrochim. Acta* 217, 16 (2016).
7. S. Hao, Y. Sun, Y. Liu, Y. Zhang, and G. Hu, *J. Alloys Compd.* 689, 587 (2016).
8. X. Bai, Q. Liu, H. Zhang, J. Liu, Z. Li, X. Jing, Y. Yuan, L. Liu, and J. Wang, *Electrochim. Acta* 215, 492 (2016).
9. J.V.S. Moreira, P.W. May, E.J. Corat, A.C. Peterlevitz, R.A. Pinheiro, and H. Zanin, *J. Electron. Mater.* 46, 929 (2017).
10. J. Ye, Z. Li, Z. Dai, Z. Zhang, M. Guo, and X. Wang, *J. Electron. Mater.* 45, 4237 (2016).
11. J.H. Kim, K.W. Nam, S.B. Ma, and K.B. Kim, *Carbon* 44, 1963 (2006).
12. Q. Yang, Z. Lu, J. Liu, X. Lei, Z. Chang, L. Luo, and X. Sun, *Prog. Nat. Sci.* 23, 351 (2013).
13. Y. Li, K. Huang, D. Zeng, S. Liu, and Z. Yao, *J. Solid State Electrochem.* 14, 1205 (2010).
14. X. Wang, X. Wu, B. Xu, and T. Hua, *J. Solid State Electrochem.* 20, 1303 (2016).
15. M. Shahraki, S. Elyasi, H. Heydari, and N. Dalir, *J. Electron. Mater.* 46, 4948 (2017).
16. A.A. Yadav, *J. Mater. Sci.: Mater. Electron.* 27, 12876 (2016).
17. A.A. Yadav, *J. Mater. Sci.: Mater. Electron.* 27, 6985 (2016).
18. S. Rajaboopathi and S. Thambidurai, *Mater. Sci. Semicond. Process.* 59, 56 (2017).
19. M. Fterich, F.B. Nasr, R. Lefi, M. Toumi, and S. Guermazi, *Mater. Sci. Semicond. Process.* 43, 114 (2016).
20. F. Cao, G.X. Pan, X.H. Xia, P.S. Tang, and H.F. Chen, *J. Power Sources* 264, 161 (2014).
21. Y. Zeng, L. Wang, Z. Wang, J. Xiao, and H. Wang, *Mater. Today Commun.* 5, 70 (2015).
22. H. Xiao, S. Yao, H. Liu, Q. Fengyu, X. Zhang, and W. Xiang, *Prog. Nat. Sci.: Mater. Int.* 26, 271 (2016).
23. M. Zhang, Q. Li, D. Fang, I.A. Ayhan, Y. Zhou, L. Dong, C. Xiong, and Q. Wang, *RSC Adv.* 5, 96205 (2015).
24. W. Yu, X. Jiang, S. Ding, and B.Q. Li, *J. Power Sources* 256, 440 (2014).
25. A.I. Inamdar, Y.S. Kim, S.M. Pawar, J.H. Kim, H. Im, and H. Kim, *J. Power Sources* 196, 2393 (2011).
26. M. Jing, C. Wang, H. Hou, Z. Wu, Y. Zhu, Y. Yang, X. Jia, Y. Zhang, and X. Ji, *J. Power Sources* 298, 241 (2015).
27. M. Krunks, J. Soon, T. Unt, A. Mere, and V. Mikli, *Vacuum* 107, 242 (2014).
28. U.M. Patil, R.R. Salunkhe, K.V. Gurav, and C.D. Lokhande, *Appl. Surf. Sci.* 255, 2603 (2008).
29. M. Jlassi, I. Sta, M. Hajji, and H. Ezzaouia, *Appl. Surf. Sci.* 308, 199 (2014).
30. K.X. Steirer, R.E. Richards, A.K. Sigdel, A. Garcia, P.F. Ndione, S. Hammond, D. Baker, E.L. Ratcliff, C. Curtis, T. Furtak, D.S. Ginley, D.C. Olson, N.R. Armstronga, and J.J. Berry, *J. Mater. Chem.* A3, 10949 (2015).
31. A.M. Soleimanpour, A.H. Jayatissaa, and G. Sumanasekera, *Appl. Surf. Sci.* 276, 291 (2013).
32. J.D. Desai, S.K. Min, K.D. Jung, and O.S. Joo, *Appl. Surf. Sci.* 253, 1781 (2006).
33. S. Zhu, Y. Dai, W. Huang, C. Zhang, Y. Zhao, L. Tan, and Z. Wang, *Mater. Lett.* 161, 731 (2015).
34. I.A. Garduno, J.C. Alonso, M. Bizarro, R. Ortega, L. Rodrıguez-Fernandez, and A. Ortiz, *J. Cryst. Growth* 312, 3276 (2010).
35. A.A. Yadav, M.A. Barote, P.M. Dongre, and E.U. Masumdar, *J. Alloys Compd.* 493, 179 (2010).
36. R. Sharma, A.D. Acharya, S.B. Shrivastava, M.M. Patidar, M. Gangrade, T. Shripathi, and V. Ganesan, *Optik* 127, 4661 (2016).
37. A.A. Yadav, E.U. Masumdar, A.V. Moholkar, K.Y. Rajpure, and C.H. Bhosale, *Phys. B* 404, 1874 (2009).
38. A.A. Yadav and U.J. Chavan, *J. Electroanal. Chem.* 782, 36 (2016).
39. A.A. Yadav, M.A. Barote, and E.U. Masumdar, *Mater. Chem. Phys.* 121, 53 (2010).
40. V. Gowthami, P. Perumal, R. Sivakumar, and C. Sanjeeviraja, *Phys. B* 452, 1 (2014).
41. Y. Li, X. Li, Z. Wang, H. Guo, and T. Li, *Ceram. Int.* 42, 14565 (2016).
42. P. Puspharajah, S. Radhakrishna, and A.K. Arof, *J. Mater. Sci.* 32, 3001 (1997).
43. A. Venter and J.R. Botha, *S. Afr. J. Sci.* 107, 1–6 (2011).
44. K.C. Yung, H. Liem, and H.S. Choy, *J. Phys. D Appl. Phys.* 42, 185002 (2009).
45. P.S. Patil and L.D. Kadam, *Appl. Surf. Sci.* 199, 211 (2002).
46. B. Sasi, K.G. Gopchandran, P.K. Manoj, P. Koshy, P.P. Rao, and V.K. Vaidyan, *Vacuum* 68, 149 (2003).
47. A.R. Balu, V.S. Nagarethinam, N. Arunkumar, and M. Suganya, *J. Electron Devices* 13, 920 (2012).
48. Y. Akaltun and T. Çayir, *J. Alloys Compd.* 625, 144 (2015).
49. A. Hakim, J. Hossain, and K.A. Khan, *Renew. Energy* 34, 2625 (2009).
50. M. Batzill and U. Diebold, *Prog. Surf. Sci.* 79, 47 (2005).
51. N. Boukmouchem, N. Azzouz, L. Bouchama, A.L. Daltin, J.P. Chopart, and Y. Bouznit, *Mater. Sci. Semicond. Process.* 27, 233 (2014).
52. S.T. Navale, V.V. Mali, S.A. Pawar, R.S. Mane, M. Naushad, F.J. Stadler, and V.B. Patil, *RSC Adv.* 5, 51961 (2015).
53. B.E. Conway, *Electrochemical Supercapacitors: Scientific Fundamentals and Technological Applications* (New York: Kluwer Academic, 1999).
54. R.R. Salunkhe, J. Lin, V. Malgras, S.X. Dou, J.H. Kim, and Y. Yamauchi, *Nano Energy* 11, 211 (2015).
55. N. Duraisamy, A. Numan, K. Ramesh, K.-H. Choi, and S. Ramesh, *Mater. Lett.* 161, 694 (2015).
56. W. Sun, L. Chen, S. Meng, Y. Wang, H. Li, Y. Han, and N. We, *Mater. Sci. Semicond. Process.* 17, 129 (2014).